# Ultrafast Uni-Traveling Carrier Photodiodes With $GaAs_{0.5}Sb_{0.5}/In_{0.53}Ga_{0.47}As$ Type-II Hybrid Absorbers for High-Power Operation at THz Frequencies

Jhih-Min Wun, Yu-Wen Wang, and Jin-Wei Shi, *Senior Member, IEEE*

***Abstract*—We demonstrate a novel type of ultrafast photodiode (PD), which offers high-power performance in the THz regime. The incorporation of a type-II $GaAs_{0.5}Sb_{0.5}$ (p)/$In_{0.53}Ga_{0.47}As$ (i) hybrid absorber in the InP-based uni-traveling carrier photodiode (UTC-PD) structure leads to an improvement in the responsivity, due to the narrowing of the bandgap and enhancement of the photo-absorption process at the type-II interface between the $GaAs_{0.5}Sb_{0.5}$ and $In_{0.53}Ga_{0.47}As$ absorption layers. Furthermore, the current blocking effect, which is usually one of the major factors limiting the output power of UTC-PDs, can be minimized due to the high-excess energy of the photo-generated electrons injected from the $GaAs_{0.5}Sb_{0.5}$ layer to the InP-based collector layer. The flip-chip bonding packaged device with an active diameter of 3 $\mu$m shows a moderate responsivity (0.11 A/W) along with a record wide 3-dB optical-to-electrical bandwidth at 0.33 THz, among all those reported for long wavelength (1.3–1.55 $\mu$m) PDs. A 13-mA saturation current and a continuous wave output power as high as –3 dBm are successfully demonstrated at an operating frequency of 0.32 THz under an optical signal with a sinusoidal envelope and a ~63% modulation depth for PD excitation.**

***Index Terms*—Photodiode, ultrafast optics.**

## I. Introduction

THE photonic millimeter-wave (MMW) generation technique has attracted interest in recent years due to its unique advantages as compared to the traditional all-electronic based solution in the MMW regime [1]. For example, by combining ultrafast photodiodes (PDs) with optical signal generation techniques, a single sweep of generated frequency from near dc to sub-THz (hundreds of GHz) becomes possible, which is useful for photonic MMW network analyzers (NA) [2], [3]. Recently, a photonic MMW source with a 0.5 THz bandwidth and a narrow linewidth (30 Hz) has been demonstrated [4].

In contrast to the traditional MMW wideband system, the photonic approach eliminates the necessity of using different metallic waveguides based frequency multipliers to cover such a wide frequency regime [5]. Ultrafast, high-power photodiodes (PDs) serve as the key components in this type of photonic MMW source, usually determining the maximum allowable operating frequency and dynamic range of the whole system [1]–[4].

Downscaling the thickness of the depletion layer and size of the device active area is essential to minimizing both the internal carrier transient time and RC-limited bandwidth in order to boost the speed of the PD up to the THz regime [6]–[11]. However, the miniaturization of the size of a sub-THz PD for THz speed performance usually results in serious device-heating and low responsivity [6]–[11] due to the high coupling loss between the input light spot and small active area of the device as well as the limited thickness of the absorption layer (~100 nm). There are two main approaches to further enhance the responsivity performance of these THz PDs. One is based on improving the geometric structure of the PD and device packaging. The responsivity can be greatly enhanced by using edge-coupled, refracting facet structures in the UTC-PD [8], [11]–[13]. It has also been demonstrated that the design of the flip-chip bonding package of the THz PD can help solve the problem of the blocking of input light by the top contact metal as well as improve both the responsivity and heat-sinking of the PD under high-power operation [9], [10]. The other approach is to modify the epi-layer structure, producing a hybrid (modified) UTC-PD [8], [14]. A $In_{0.53}Ga_{0.47}As$ based p-type partially depleted absorber (PDA) layer is adopted to reduce the probability of electron recombination in the p-type layer and enhance the internal quantum efficiency [8], [14].

In this work, we demonstrate a novel UTC-PD with a type-II PDA layer and a flip-chip bonding package designed to further enhance its efficiency, device heat-sinking, and output saturation power at the THz regime. By using the type-II (p-$GaAs_{0.5}Sb_{0.5}$/i- $In_{0.53}Ga_{0.47}As$) PDA in our device, the internal absorption process and responsivity performance can be improved due to the narrowing of the effective bandgap [15] in the type-II hetero-structure. Furthermore, the injection of photo-generated electrons with high excess energy from the p-$GaAs_{0.5}Sb_{0.5}$ layer can effectively minimize the current blocking effect at the collector layer [16]. The device has a reasonable responsivity (0.11 A/W) and with it we can attain a record wide 3-dB O-E bandwidth at 0.33 THz, the largest

Manuscript received May 24, 2017; revised July 19, 2017 and August 14, 2017; accepted August 14, 2017. Date of publication August 21, 2017; date of current version August 29, 2017. This work was supported in part by the Ministry of Science and Technology in Taiwan under Grant 105-2622-E-008-014-CC2, and in part by the Asian Office of Aerospace Research and Development under Grant FA2386-17-1-0033. *(Corresponding Author: Jin-Wei Shi.)*

The authors are with the Department of Electrical Engineering, National Central University, Taoyuan 320, Taiwan (e-mail: p3984011@hotmail.com; a072222685@yahoo.com.tw; jwshi@ee.ncu.edu.tw).

Color versions of one or more of the figures in this paper are available online at http://ieeexplore.ieee.org.

Digital Object Identifier 10.1109/JSTQE.2017.2741106

1077-260X © 2017 IEEE. Personal use is permitted, but republication/redistribution requires IEEE permission.
See http://www.ieee.org/publications_standards/publications/rights/index.html for more information.

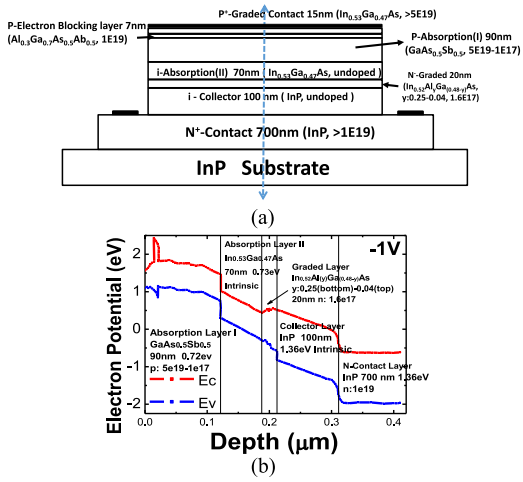


Fig. 1. (a) Conceptual cross-sectional view of the device. (b) Simulated band diagram of the demonstrated hybrid-absorber UTC-PDs under $-1$ V bias voltage. The unit for doping density in each layer is $cm^{-3}$.

among those reported for PDs operated at telecommunication wavelengths (1.3–1.55 $\mu$m) [8], [17]. In addition, the device demonstrates a high continuous wave (CW) output power of $-3$ dBm (13 mA output photocurrent) at an operating frequency of 0.32 THz, under excitation by an optical signal with a sinusoidal envelope and a ~63% modulation depth emitted from a two-laser heterodyne-beating system.

## II. Design of the Device Structure and Fabrication

Fig. 1(a) and (b), respectively, show a conceptual cross-sectional view and the simulated band diagram of our demonstrated device structure. Our epi-layer structure was grown on the semi-insulating (S.I.) InP substrate in a molecular-beam epitaxy (MBE) chamber.[1] As can be seen, the hybrid absorption region with a type-II band alignment ($GaAs_{0.5}Sb_{0.5}$/$In_{0.53}Ga_{0.47}As$) is comprised of two major parts [15]. One is the p-type $GaSb_{0.5}As_{0.5}$ absorption layer with a thickness of 90 nm and a graded doping profile (top: $5 \times 10^{19}$ $cm^{-3}$ to bottom: $1 \times 10^{17}$ $cm^{-3}$) designed to accelerate the electron diffusion process. The other is an intrinsic $In_{0.53}Ga_{0.47}As$ layer with a thickness of 70 nm. This type of undoped $In_{0.53}Ga_{0.47}As$ layer is used in the p-type absorber of the traditional UTC-PD to minimize the electron recombination process. Although such an intrinsic layer may contribute to undesired hole transport, the corresponding transit time limited bandwidth of the holes is still as high as 0.5 THz, larger than the measured net O-E bandwidth of our device (~0.33 THz), which will be discussed in greater detail later.

Furthermore, the type-II band alignment between the interface of the $GaAs_{0.5}Sb_{0.5}$ and $In_{0.53}Ga_{0.47}As$ layers narrows the effective bandgap to 0.5 eV (~2.4 $\mu$m cut-off wavelength [15]), which can further enhance the absorption process under 1.55 $\mu$m (0.8 eV) wavelength excitation. Our collector layer consists of an intrinsic InP layer with an ultra-low background doping density in order to reduce the required bias voltage and device heating under high power operation [16]. A thin (20 nm) n-type charge layer, with a $In_xAl_yGa_{1-x-y}As$ (x: 0.52; y: 0.04 to 0.25) graded bandgap structure, is inserted between the intrinsic (i) -$In_{0.53}Ga_{0.47}As$ and i-InP layers. The result is a drop in the electron potential and further suppression of the current blocking effect [10], [14]. Fig. 2(a) to (c) shows a top-view of the active PD chip, the co-planar waveguide (CPW) pad on the AlN substrate in the flip-chip bonding package, which can provide a nearly ~400 GHz 3-dB bandwidth [10], and the PD chip after flip-chip bonding packaging, respectively. PDs with three different active diameters of 3, 5, and 8 $\mu$m (devices A to C) were fabricated. For details of the PD fabrication process please refer to our previous work [10]. After the deposition of an anti-reflective (AR) coating on the back-side of the chip, the measured DC responsivity was around 0.14 A/W for devices B and C. When the device active diameter was downscaled to 3 $\mu$m (device A), there was a degradation in the responsivity to 0.11 A/W due to the coupling and diffraction loss between the optical beam and device active mesa. We obtained larger values for the DC responsivity than in our previous work with an ultra-fast UTC-PD (~0.11 vs. <0.1 A/W) with a whole p-type $In_{0.53}Ga_{0.47}As$ absorber of the same thickness (~160 nm) and the same flip-chip bonding package [9], [10]. This results suggest that our proposed type-II hybrid absorber design can effectively improve the responsivity performance of THz UTC-PDs with a thin $In_{0.53}Ga_{0.47}As$ absorption layer.

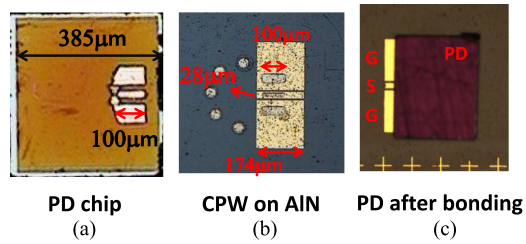


Fig. 2. Top-views of the active PD chip (a), bonding pads on the AlN substrate (b), and PD chip after flip-chip bonding (c).

## III. Measurement Results

A heterodyne beating system was used to measure the dynamic performance of the fabricated device structure. A power meter with a sensor head which covers from dc to 50 GHz, was used for measurement in this frequency range. When the measurement frequency was greater than 75 GHz, a thermal MMW power meter (PM4, VDI-Erickson), which could cover the 75 GHz to THz measurement frequency regime, was used. The maximum measurement bandwidth for our system was limited by the WR-3.4 waveguide based MMW probe which operated at around 325 GHz.

From dc to 50 GHz, the frequency dependent loss arising from the passive components will mainly originate from the radio-frequency (RF) probe, coaxial cable, and bias tee, typically at around 3 dB at 50 GHz operation. The value of the frequency dependent loss has been carefully verified using a broadband network analyzer (0.01 to 67 GHz). In our setup, with a further

[1] **Intelligent Epitaxy Technology, Inc.,** 1250 E Collins Blvd, Richardson, TX 75081.

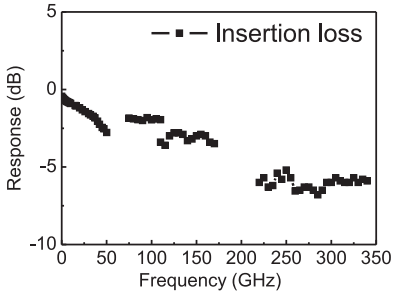


Fig. 3. The frequency response of insertion loss in our hetero-dyne beating measurement system.

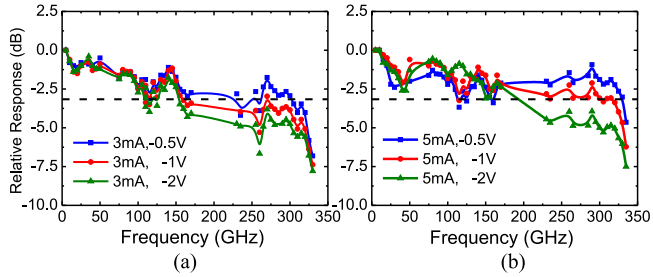


Fig. 4. Bias dependent O-E frequency responses measured under different output photocurrents: (a) 3 mA and (b) 5 mA for device A with a 3 $\mu$m active diameter.

increase in the measurement frequency (75–325 GHz), there are three major sources of insertion loss. The first is the frequency dependent insertion loss from the waveguide probe. For the WR-3.4 waveguide probe, the loss is around 5 dB at around 300 GHz operation according to value provided by the manufacturer of the waveguide probe.[2] The second is the loss associated with the straight WR-10 waveguide section (0.6 dB at 300 GHz)[3], which is connected with the power sensor head. The last is from the waveguide taper (0.3 dB at 300 GHz).[3] This component connects the sensor head of thermal power meter, which has a WR-10 waveguide as input port, with the head of the waveguide probes (WR-3.4 or WR-6). Fig. 3 shows the total frequency response (from dc to 325 GHz) of the insertion loss in our measurement setup. Although there are two gaps (50–75 GHz and 170–220 GHz) in the frequency range of interest (dc to 325 GHz), this should not have any influence on the accuracy of the measurement as following discussion.

All the dynamic measurement results presented here, which include the O-E frequency responses and THz output power, have been carefully de-embedded to remove the insertion loss as based on the figure. In addition, during our O-E frequency response measurement across such a wide bandwidth (near dc to 325 GHz), we have tried to keep the optical modulation depth as a constant at around 63% by tuning the polarization states of the light sources during the heterodyne beating process. By comparing the actually measured photo-generated RF power from a reference PD,[4] which has an over 100 GHz 3-dB O-E bandwidth, with its theoretical output power under a 100% optical modulation depth, we can estimate the optical modulation depths of our light source from near dc to around 110 GHz operating frequency. On the other hand, although we don't have any good reference PD to extract the values of modulation depth when the measurement frequency reaches 220–325 GHz, the corrected output power at the different bands (dc to 50 GHz, 75–110 GHz, 110–170 GHz, and 220–325 GHz) can be stitched together very well under such the same value of optical modulation depth ($\sim$63%) characterized at low-frequency (dc to 110 GHz). These results indicate the validness and accuracy of our speed and power measurement processes, which will be discussed latter in the measured O-E frequency responses.

Figs. 4 to 6 show the measured bias dependent O-E frequency responses under different output photocurrents at 3 and 5 mA for devices A to C, respectively. As can be seen in Fig. 3, the optimum bias for high-speed performance happens at $-0.5$ V under output photocurrents of 3 and 5 mA. A further increase in the reverse bias voltage to $-2$ V would result in degradation of the O-E bandwidth, which can be attributed to the electron inter-valley scattering effect under a high applied electric field [8], [10]. In addition, under the same reverse bias, a slight bandwidth enhancement can be observed when the output photocurrent increases from 3 to 5 mA. This phenomenon, which usually happens in UTC-PDs [7], can be attributed to the self-induced field of photo-generated holes in the p-type absorber, which can accelerate the electron diffusion process and enhance the net O-E bandwidth of the PD. As shown in Fig. 4(b), for device A, under an output photocurrent of 5 mA, an optimum bias of $-0.5$ V, and a load of 50 $\Omega$, the maximum 3-dB O-E bandwidth can reach 0.33 THz. Although there are two dips (at 115 GHz and 160 GHz) shown in the trace, the values are pretty close to the $-3$ dB line ($\sim -3.7$ dB) so should not have any significant influence on practical applications. This bandwidth is the highest ever reported for ultrafast PDs for operation at telecommunication wavelengths (1.3 to 1.55 $\mu$m) [7], [8], [10], [17].

Our epi-layer structure is designed to achieve ultra-fast performance with a near THz bandwidth. A thinner depletion layer thickness ($\sim$190 nm) is thus adopted to shorten the internal carrier transit time, which in turn results in a small RC-limited bandwidth when the device active area is enlarged.

As shown in Figs. 5 and 6, there is a degradation in the 3-dB O-E bandwidth to around 150 and 60 GHz for devices B and C, respectively. In contrast to device A, when operating at the THz regime ($\sim$0.33 THz), the optimum bias for high-speed performance of device C shifts from $-0.5$ to $-2$ V. This indicates a gradual enhancement in the RC-limited bandwidth by the increase in the reverse bias voltage due to the widening of the depletion region, rather than the measured net O-E bandwidth being dominated by the internal carrier transit time.

The equivalent-circuit modeling technique was used to extract the RC-limited bandwidth for each device structure [10]; see Fig. 7(a). Here, the "PAD Simulation" section of the table shows the simulated scattering (S) parameters of the co-planar

[2]**GGB Industries, Inc.,** P.O. BOX 10958, NAPLES, FL 34101.

[3]**Virginia Diodes, Inc.,** 979 Second Street, S.E. Suite 309, Charlottesville, VA 22902-6172. VDI APPLICATION NOTE: Power Measurement above 110 GHz.

[4]**Finisar,** 1389 Moffett Park Drive, Sunnyvale, CA 94089. Product: XPDV4121R.

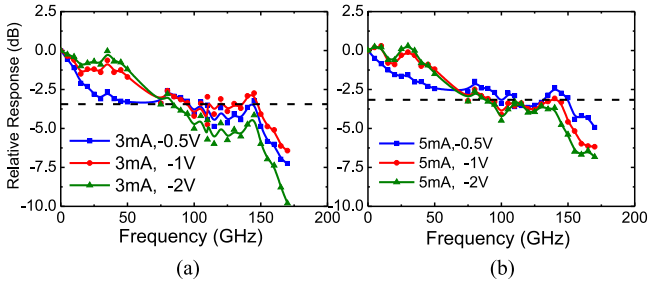


Fig. 5. Bias dependent O-E frequency responses measured under different output photocurrents: (a) 3 mA and (b) 5 mA for device B with a 5 $\mu$m active diameter.

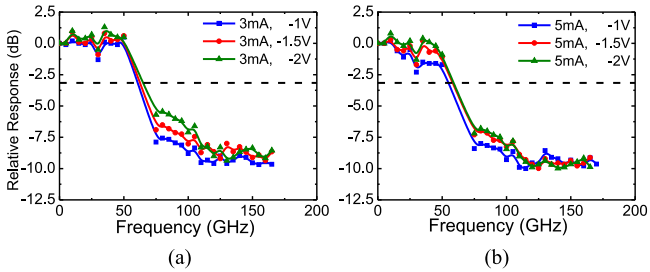


Fig. 6. Bias dependent O-E frequency responses measured under different output photocurrents: (a) 3 mA and (b) 5 mA for device C with an 8 $\mu$m active diameter.

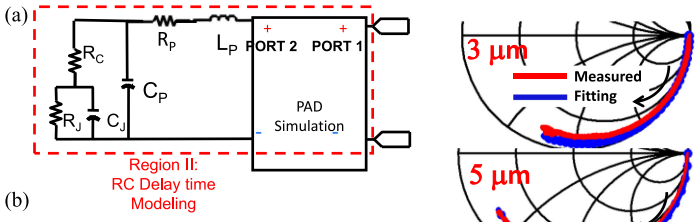


| | Physical Meaning | 3 μm | 5 μm | 8 μm |
|---|---|---|---|---|
| Cj | Junction Capacitance (fF) | 4.4 | 14.8 | 25.5 |
| Rj | Junction Resistance (kΩ) | >100 | >100 | >100 |
| Rp | Parasitic Resistance (Ω) | 1.5 | 5 | 4 |
| Rc | Contact Resistance (Ω) | 109 | 92 | 40 |
| Cp | Parasitic Capacitance (fF) | 7.9 | 16.4 | 16.4 |
| Lp | Parasitic Inductance (pH) | 0.09 | 0.01 | 0.01 |
| PAD Simulation | The simulated S-parameters for PAD by using HFSS software | | | |

Fig. 7. (a) Equivalent-circuit-model; (b) measured (continuous line) and fitted (open circles) $S_{11}$ parameters from near dc to 65 GHz under a fixed dc bias ($-1$ V) for devices A to C, with different active diameters of 3, 5, and 8 $\mu$m. The black arrowhead indicates the increase in the sweep frequency. The table shows the values of the circuit elements used in the modeling process. HFSS: high frequency structural simulator (ANSYS, Inc., Southpointe, 275 Technology Drive, Canonsburg, PA 15317, USA.)

waveguide (CPW) used in our device; see also Fig. 2(b). The values used in the fitting process are shown in the table in Fig. 7(b). The measured and simulated frequency responses for the microwave reflection coefficient parameter ($S_{11}$) under a $-1$ V bias voltage for devices A to C are shown; see the Smith chart. Clearly, there is a good match between the simulated and measured results from 100 MHz to 65 GHz.

Based on the established equivalent circuit model, we can thus extract the RC-limited frequency responses for each device, indicated by the solid lines in Fig. 8. The frequency response

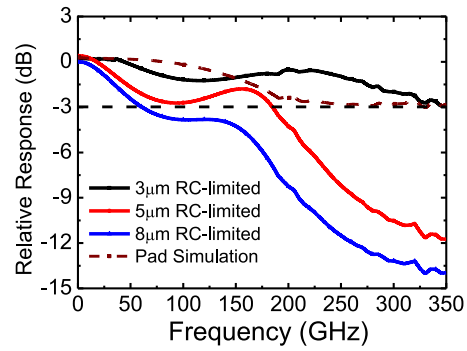


Fig. 8. The extracted RC-limited frequency responses for devices A to C.

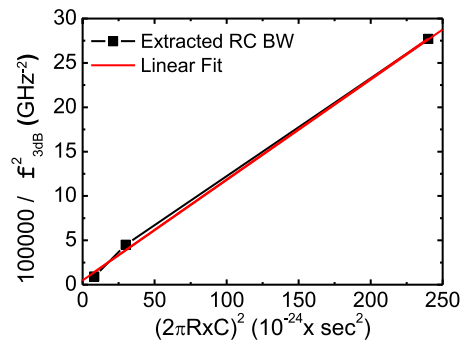


Fig. 9. The extracted $(1/f_{\mathrm{RC}})^2$ versus the measured $(10^5/f_{3\mathrm{dB}}^2)$for devices A to C.

for the "PAD Simulation" is also given in this figure for reference. We can clearly see that due to the existence of parasitic inductance ($L_p$) and capacitance ($C_p$) in the equivalent circuit model, there is an extra resonant frequency in the traces of the RC-limited frequency response as compared to those for the "Pad Simulation". In addition, it can be seen that after aggressively downscaling the active diameter of the device from 8 to 3 $\mu$m, a significant increase of RC-limited bandwidth from 60 to 350 GHz can be observed. As shown in the table in Fig. 7(b), although reducing the active diameter will lead to an increase in the contact resistance ($R_c$; 40 to 109 Ω), we still get a net increase in the RC-limited bandwidth. This is because during calculation of the RC-bandwidth, a fixed load of 50 Ω must be included regardless of the change in the active diameter ($R_c$) of the device. The junction capacitance ($C_j$) thus plays a more important role in determining the RC-limited bandwidth of the device.

The overall O-E 3-dB bandwidth $(f_{3\mathrm{dB}})$ of a PD is determined by the carrier transport time $(1/f_t)$ and the RC time constant $(1/f_{\mathrm{RC}})$. In order to investigate the internal carrier transport time inside our device, the following equation is adopted [18]:

$$\frac{1}{f_{3\mathrm{dB}}^2} = \frac{1}{f_{\mathrm{RC}}^2} + \frac{1}{f_t^2} \tag{1}$$

Using the extracted RC-limited bandwidths and the measured net O-E bandwidths, as shown in Figs. 8 and 4–6, respectively, we can thus obtain the internal transit time inside our device.

Fig. 9 shows the $(1/f_{\mathrm{RC}})^2$ vs.$(10^5/f_{3\mathrm{dB}}^2)$ values for devices A to C with three different active diameters (3, 5, and 8 $\mu$m). With

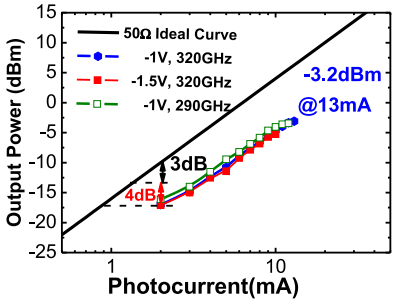


Fig. 10. The measured photo-generated MMW power versus photocurrent for device A with a 3 $\mu$m active diameter under sinusoidal signal excitation and with different reverse biases at operating frequencies of 0.32 and 0.29 THz. The solid line shows the ideal trace for a 100% optical modulation depth and 50 Ω load.

(1), the internal carrier transient time in our device is determined using the intercepts shown along the y-axis of this figure. The obtained $f_t$ can be as high as 470 GHz. The drift-diffusion model is used to estimate the transit time limited bandwidth [19]. The extracted electron drift-velocity through the 100 nm InP collector layer is around $7 \times 10^5$ m/sec. The dominating factor for the total transit time inside our proposed epi-layer structure should be the drift-time of the photo-generated electrons/holes through the depleted 70 nm thick $In_{0.53}Ga_{0.47}As$ absorption layer. Due to the fact that this layer is fully depleted and there is no p-type background doping, the transit time of photo-generated holes across such layer plays an important role in determining the total transit time in our device. The average drift-velocity of electrons and holes across this layer is around $1 \times 10^5$ m/sec, which is higher than the value reported ($5.3 \times 10^4$ m/sec) for $In_{0.53}Ga_{0.47}As$ p-i-n PDs [6]. The extracted drift-velocity numbers suggest that non-equilibrium electron transport plays an import role in the proposed epi-layer structure [20] for THz operation. The phenomenon of non-equilibrium electron transport usually happens in the case of electrons with high excess energy during transportation and the carrier drift-distance is close to (or less than) the electron mean free path. This leads to a reduction in the probability of carrier collision and a much faster effective carrier drift-velocity than that obtained under steady-state measurement, as has usually been reported. The results of a Monte Carol simulation show that it is possible to obtain an electron drift-velocity as high as around $6 \times 10^5$ m/sec in the collector layer of InP based UTC-PDs [20].

Fig. 10 shows the measured photo-generated MMW power versus output photocurrent for device A obtained under different reverse biases ($-1$ and $-1.5$V) with the two-laser heterodyne-beating setup. The measurement frequency chosen was around the 3-dB O-E bandwidth at 320 GHz and 290 GHz. The ideal relation between the MMW power and averaged photocurrent (solid line) with a 100% optical modulation depth under a 50 Ω load is also plotted for reference. We can clearly see that the saturation current of device A under $-1$ V bias is around 13 mA and the corresponding maximum output power is around $-3$ dBm at an operating frequency of 0.32 THz. When the reverse bias voltage is further increased to $-1.5$ V, the maximum output current is limited by thermal failure. In addition, there is a total 7 dB difference between the measured and ideal photo-generated THz power, under the same amount of output photocurrent, as specified in this figure. This 7 dB discrepancy mainly arises from two factors. One is the nearly 3-dB high-frequency roll-off from the PD itself, when operated at near its 3-dB bandwidth (0.33 THz) frequency point. As can be seen, under the same output photocurrent, the output power measured at a frequency of 0.29 THz is around 1 dB larger than that measured at 0.32 THz. This is because of the approximately 1 dB difference in magnitude between the measured O-E responses at these two frequencies (0.29 and 0.32 THz), as shown in $-1$ V trace of Fig. 4(b). The other 4 dB loss originates from the optical modulation depth in our two-laser heterodyne-beating system at the near THz frequency separation being only around 63%. Due to the wide separation (>2.4 nm) between the two optical central wavelengths and the non-flat gain spectrum of the high-power erbium-doped optical fiber amplifier (EDFA) used, the two wavelengths have different reference levels of amplified spontaneous emission (ASE) noise in their spectra, which may lead to degradation of the optical modulation depth of the THs signal during the hetero-dyne beating process. By using an optical pulse train with the same THz repetition rate as the light source for device excitation, a larger optical modulation depth with a higher maximum output power from PD can be expected [10].

The performance of the new device is compared with that of our previously reported ultrafast THz-regime UTC-PDs with a pure $In_{0.53}Ga_{0.47}As$ absorber layer. They are excited using the same two-laser heterodyne-beating setup with a close value of optical modulation depth (~63%) [10].

The comparison shows that both devices exhibit similar output power (around -3 dBm) and saturation current (12 vs. 13 mA) values. However, it is demonstrated that the new device A, with the type-II hybrid absorber, can be operated at a higher frequency (0.32 vs. 0.28 THz) due to its larger O-E bandwidth (0.33 vs. 0.315 THz) [10]. The device modeling results [10] show that both the previously reported UTC-PD and device A exhibit the same RC-limited bandwidth of 0.35 THz. The faster speed performance of device A can thus be attributed to the shortening of the internal carrier transit time.

Using the obtained saturation current (>13 mA) and the simulated electric-field inside the depleted region of our device under $-1$ V bias, as discussed in Fig. 1, we estimate the electron drift-velocity ($V_e$) across the depletion region. The formula used for calculation of the space charge field ($E_{SCS}$) induced by the drifting of electrons in the depletion layer is [6]

$$E_{scs} = J\left(\frac{D}{\varepsilon V_e}\right) \tag{2}$$

where D indicates the total depletion layer thickness (190 nm), which includes the 70 nm $In_{0.53}Ga_{0.47}As$, 20 nm graded bandgap layer and 100 nm InP collector layer; J is the output photocurrent density; $\varepsilon$ is the dielectric constant of InP; and $V_e$ is the drift-velocity of the electrons. The simulated E-field inside the 100 nm InP collector layer is around 60 kV/cm under $-1$ V bias. By assuming that the minimum net E-field over 10 kV/cm inside the collector layer under an output current of

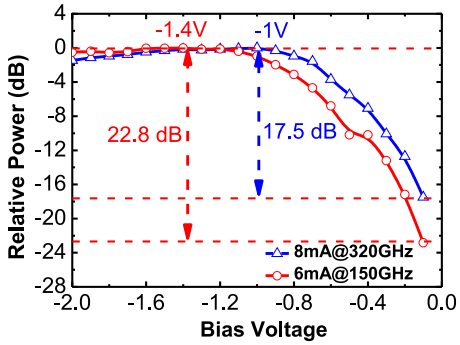


Fig. 11. The measured transfer curve (bias voltage vs. output THz power) of device A at 0.15 (red lines) and 0.32 (blue line) THz. Each trace is normalized to its own maximum power at the different reverse bias voltages (−1 and −1.4V), as specified.

13 mA and bias current of −1 V, the corresponding value of $V_e$ must be over $6 \times 10^5$ m/sec, as calculated with (1) [9], [10]. This value is consistent with the extracted electron drift-velocity illustrated in Fig. 9. Both the O-E responses and saturation current measurement results strongly support the conclusion that our proposed epi-layer structure can really provide the ultrafast non-equilibrium electron transport [20] needed to further break the bottleneck of the transit time limited bandwidth inside UTC-PDs for THz operation.

The fast bias modulation characteristic of the high-power PD is important for applications in photonic wireless communication [21]–[24], especially for the case of short-pulse train excitation [24]. By using the bias modulation technique for PDs for remote-up conversion, the direct on-off keying (OOK) modulation of the optical pulse train can be eliminated. This would solve the problem of serious chromatic dispersion in a modulated optical pulse train during fiber transmission [24]. However, near forward bias operation of UTC-PDs is necessary to quench the photo-generated THz power, which would seriously limit the modulation speed [25]. In previous work, we demonstrated that, by the incorporation of an additional p-type charge layer inside the collector layer of a UTC-PD (NBUTC-PD), the operation window would shift to the reverse bias regime, allowing ultrafast bias modulation performance (>25 Gbit/sec) for photonic wireless communication [24], [26].

Fig. 11 shows the measured transfer curve (bias voltage versus photo-generated MMW power on a linear scale) of device A at operating frequencies of 0.15 and 0.32 THz. Each trace is normalized to the value of its own maximum output power at different reverse biases (−1.4 and −1 V), as specified in the figure. We can clearly see that a nearly 20 dB swing in THz output power can be achieved when the bias voltage swings from zero to −1 V. Such a significant change in the THz power at the reverse bias regime can be attributed to the insertion of an n-type charge layer in the collector layer, as illustrated in Fig. 1(b). When the reverse bias voltage is less than −1 V, the charge layer is not depleted, resulting in a small electric-field inside the collector layer. This slows down the electron drift-velocity in the collector layer, causing a degradation in the speed performance of the device, and quenching the photo-generated THz power. The characteristic of very-fast switching of the THz power can be expected in our device due to the elimination of forward bias operation and variation in output photocurrent [26].

## IV. Conclusion

In conclusion, we demonstrate a novel UTC-PD structure with further improved speed and responsivity performance for THz operation. Through the use of type-II hybrid absorber layer and improved flip-chip bonding package we produce a PD which exhibits a reasonable responsivity of 0.11 A/W and a record-wide O-E bandwidth (0.33 THz), among all those reported for ultrafast PDs to be used at telecommunication wavelengths. A saturation current of over 13 mA and a high CW output power of −3 dBm at 0.32 THz are successfully demonstrated under excitation by an optical sinusoidal signal with a ∼63% modulation depth, generated by a two-laser heterodyne beating system. The dynamic measurement and modeling results reveal that ultrafast non-equilibrium electron transport plays an important role in the speed performance of this PD. The device with this structure also exhibits excellent bias modulation characteristics, i.e., an extremely small driving voltage (0 to −1 V) with a nearly 20 dB swing of THz power.

## References

[1] A. Stöhr *et al.*, "Millimeter-wave photonic components for broadband wireless systems," *IEEE Trans. Microw. Theory Tech.*, vol. 58, no. 11, pp. 3071–3082, Nov. 2010.

[2] T. Nagatsuma *et al.*, "1.55-$\mu$m photonic systems for microwave and millimeter-wave measurement," *IEEE Trans. Microw. Theory Tech.*, vol. 49, no. 10, pp. 1831–1839, Oct. 2001.

[3] S. Preu, "Components towards a photonics aided THz vector network analyzer," in *Proc. 2016 Int. Conf. Opt. Fiber Commun.*, Anaheim, CA, USA, Mar. 2016, Paper no. W4K.4.

[4] A. Hallal, S. Bouhier, and F. Bondu, "Synthesis of a 30-Hz linewidth wave tunable over 500 GHz," *IEEE Trans. Microw. Theory Tech.*, vol. 65, no. 4, pp. 1367–1371, Apr. 2017.

[5] G. Chattopadhyay, "Technology, capabilities, and performance of low power terahertz sources," *IEEE Trans. THz Sci. Technol.*, vol. 1, no. 1, pp. 33–53, Sep. 2011.

[6] K. Kato, "Ultrawide-band/high-frequency photodetectors," *IEEE Trans. Microw. Theory Tech.*, vol. 47, no. 7, pp. 1265–1281, Jul. 1999.

[7] H. Ito *et al.*, "High-speed and high-output InP-InGaAs unitraveling-carrier photodiodes," *IEEE J. Sel. Topics Quantum Electron.*, vol. 10, no. 4, pp. 709–727, Jul./Aug. 2004.

[8] T. Ishibashi, Y. Muramoto, T. Yoshimatsu, and H. Ito, "Unitraveling-carrier photodiodes for terahertz applications," *IEEE J. Sel. Topics Quantum Electron.*, vol. 20, no. 6, Nov./Dec. 2014, Art. no. 3804210.

[9] J.-W. Shi, F.-M. Kuo, and J. E. Bowers, "Design and analysis of ultra-high speed near-ballistic uni-traveling-carrier photodiodes under a 50 Ω load for high-power performance," *IEEE Photon. Technol. Lett.*, vol. 24, no. 7, pp. 533–535, Apr. 2012.

[10] J.-M. Wun *et al.*, "Photonic high-power CW THz-wave generation by using flip-chip packaged uni-traveling carrier photodiode and femtosecond optical pulse generator," *IEEE/OSA J. Lightw. Technol.*, vol. 34, no. 4, pp. 1387–1397, Feb. 2016.

[11] E. Rouvalis, C. C. Renaud, D. G. Moodie, M. J. Robertson, and A. J. Seeds, "Traveling-wave uni-traveling carrier photodiodes for continuous wave THz generation," *Opt. Express*, vol. 18, no. 11, pp. 11105–11110, May 2010.

[12] Y. Muramoto, H. Fukano, and T. Furuta, "A Polarization-independent refracting-facet uni-traveling-carrier photodiode with high efficiency and large bandwidth," *IEEE/OSA J. Lightw. Technol.*, vol. 24, no. 10, pp. 3830–3834, Oct. 2006.

[13] X. Xie *et al.*, "High-power and high-speed heterogeneously integrated waveguide-coupled photodiodes on silicon-on-insulator," *IEEE/OSA J. Lightw. Technol.*, vol. 34, no. 1, pp. 73–78, Jan. 2016.

[14] Z. Li, H. Pan, H. Chen, A. Beling, and J. C. Campbell, "High-saturation current modified uni-traveling-carrier photodiode with cliff layer," *IEEE J. Quantum Electron.*, vol. 46, no. 5, pp. 626–632, May 2010.
[15] R. Sidhu *et al.*, "2.4 $\mu$m cutoff wavelength avalanche photodiode on InP substrate," *Electron. Lett.*, vol. 42, no. 3, pp. 181–182, 2006.
[16] J.-M. Wun, R.-L. Chao, Y.-W. Wang, Y.-H. Chen, and J.-W. Shi, "Type-II GaAs0.5Sb0.5/InP uni-traveling carrier photodiodes with sub-THz bandwidth and high-power performance under zero-bias operation," *IEEE/OSA J. Lightw. Technol.*, vol. 35, no. 4, pp. 711–716, Feb. 2017.
[17] H. Ito, T. Furuta, S. Kodama, N. Watanabe, and T. Ishibashi "Inp/InGaAs uni-travelling-carrier photodiode with 310GHz bandwidth," *Electron. Lett.*, vol. 36, pp. 1809–1810, Oct. 2000.
[18] J.-W. Shi, K.-L. Chi, C.-Y. Li, and J.-M. Wun, "Dynamic analysis of high-efficiency InP based photodiode for 40 Gbit/sec optical interconnect across a wide optical window (0.85 to 1.55 $\mu$m)," *IEEE/OSA J. Lightw. Technol.*, vol. 33, no. 4, pp. 921–927, Feb. 2015.
[19] J.-W. Shi and C.-W. Liu, "Design and analysis of separate-absorption-transport-charge-multiplication traveling-wave avalanche photodetectors," *IEEE/OSA J. Lightw. Technol.*, vol. 22, no. 6, pp. 1583–1590, Jun. 2004.
[20] T. Ishibashi, "Nonequilibrium electron transport in HBTs," *IEEE Trans. Electron. Devices*, vol. 48, no. 11, pp. 2595–2604, Nov. 2001.
[21] S. Koenig *et al.*, "Wireless sub-THz communication system with high data rate," *Nature Photon.*, vol. 7, pp. 977–981, Dec. 2013.
[22] J.-W. Shi, C.-B. Huang, and C.-L. Pan, "Millimeter-wave photonic wireless links for very-high data rate communication," *NPG Asia Mater.*, vol. 3, no. 2, pp. 41–48, Apr. 2011.
[23] H.-J. Song and T. Nagatsuma, "Present and future terahertz communications," *IEEE Trans. THz Sci. Technol.*, vol. 1, no. 1, pp. 256–263, Sep. 2011.
[24] F.-M. Kuo *et al.*, "Remotely up-converted 20 Gbit/s error-free wireless on-off-keying data transmission at W-band using an ultra-wideband photonic transmitter-mixer," *IEEE Photon. J.*, vol. 3, no. 2, pp. 209–219, Apr. 2011.
[25] A. Hirata, T. Furuta, H. Ito, and T. Nagatsuma, "10-Gb/s millimeter-wave signal generation using photodiode bias modulation," *IEEE/OSA J. Lightw. Technol.*, vol. 24, no. 4, pp. 1725–1731, Apr. 2006.
[26] N.-W. Chen, J.-W. Shi, F.-M. Kuo, J. Hesler, T. W. Crowe, and J. E. Bowers, "25 Gbits/sec error-free wireless link between Ultra-Fast W-Band photonic transmitter-mixer and envelop detector," *Opt. Express*, vol. 20, no. 19, pp. 21223–21234, Sep. 2012.

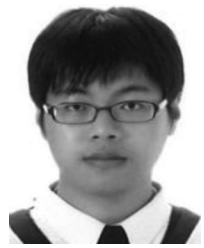

**Jhih-Min Wun** was born in Taoyuan, Taiwan on October 3, 1988. He is currently working toward the Ph.D. degree in the Department of Electrical Engineering, National Central University, Taoyuan. His current research interests include high-speed optoelectronic device measurement and sub-THz high-speed photodiodes.

**Yu-Wen Wang** was born in Kaohsiung, Taiwan, on November 3, 1992. He is currently working toward the Master's degree in the Department of Electrical Engineering, National Central University, Taoyuan, Taiwan. His current research interests include high-speed and high-power photodiodes.

**Jin-Wei Shi** (M'03–SM'12) was born in Kaohsiung, Taiwan on January 22, 1976. In 2003, he joined the Department of Electrical Engineering, National Central University, Taoyuan, Taiwan, where he has been serving as a Professor since 2011. In 2011–2012 and again in 2016, he joined the ECE Department of UCSB as a Visiting Professor. His current research interests include ultrahigh speed/power photodetectors, electro-absorption modulators, THz photonic transmitters, and VCSELs. He has authored or coauthored more than 4 book chapters, 120 Journal papers, 180 conference papers, and holds 30 patents. He received the Da-You Wu Memorial Award in 2010.